Ultrastructural Study of Plasmodesmata in the Brown Alga *Dictyota dichotoma* (Dictyotales, Phaeophyceae)

Makoto Terauchi[1, 2], Chikako Nagasato[2], Naoko Kajimura[3],
Yoshinobu Mineyuki[4], Kazuo Okuda[5], Christos Katsaros[5], Taizo Motomura[2]

[1] Graduate School of Environmental Science, Hokkaido University, Sapporo 060-0810, Japan

[2] Muroran Marine Station, Field Science Center for Northern Biosphere, Hokkaido University, Muroran 051-0003, Japan

[3] Research Center for Ultra-High Voltage Electron Microscopy, Osaka University, Osaka 567-0047, Japan

[4] Department of Life Science, Graduate School of Life Science, University of Hyogo, Himeji 671-2280, Japan

[5] Graduate School of Kuroshio Science, Kochi University, 2-5-1, Kochi 780-8520, Japan

[6] Department of Botany, Faculty of Biology, University of Athens, Athens 157 84, Greece

Abstract

Plasmodesmata (PD) singular: plasmodesma, from the Greek *plasma*=cytoplasm and *desmos*=connection) are intercellular bridges of multicellular plants, directly connecting cytoplasms of neighboring cells. They play a crucial role in cell-to-cell communication and cell development. Although brown algae (Phaeophyceae, Heterokontophyta) are phylogenetically far from the lineage of land plants, they possess a complex multicellularity with PD like green plants. In this study, the ultrastructure and the formation of PD in the brown alga *Dictyota dichotoma*, were studied using transmission electron microscopy (TEM) and electron tomography with rapid freezing and freeze-substitution. *D. dichotoma*, possesses plasma membrane-lined simple PD without an internal endoplasmic reticulum (ER) (desmotubule), different from those of land plants. PD were clustered in thin cell wall regions forming pit fields. Fine proteinaceous internal bridges were observed in the cavity. Ultrastructural observations of cytokinesis of *D. dichotoma* revealed that the PD formation started from an early stage of cytokinesis with the formation of tubular pre-plasmodesmata (PPD) within the membranous sacs (MSs) of the cytokinetic diaphragm. Clustering of these PPD became into the future pit field. As cytokinesis proceeds, electron-dense material extended from the outer surface of the middle part of PPD and finally formed the nascent cell wall. From these results, it is suggested that PPD would be associated with the cell wall development during cytokinesis of *D. dichotroma*.

Keywords

Brown algae・Cytokinesis・Electron tomography・Plasmodesmata

Introduction

Among the diverse organisms, only a few groups have evolved to gain a complex multicellularity. Brown algae (Phaeophyceae) are a member of the multicellular organisms that evolved in aquatic environment and are phylogenetically distant from the other multicellular groups such as animals, fungi, green plants and red algae (Yoon et al. 2004). They are dominant in the coastal environment, forming the seaweed forests which give good habitats to aquatic animals, and contributing to the ocean carbon fixation.

In the multicellular organisms, the cell-to-cell communication plays a crucial role in the organized development and differentiation. Those important biological processes can be achieved by the intercellular connections, through which the traffic of photosynthetic products and variable signal molecules takes place. It is well-known that intercellular connections structurally vary among the multicellular organisms. Animal cells have gap junctions which consist of a complex of connexin family proteins (Makowski et al. 1984, Kumar and Gilula 1996). They connect cytoplasms of adjacent cells and give way to transport of ions and small molecules. In plants including algae, it has been well known that various types of cytoplasmic interconnection occur between cells (Marchant 1976). Red algae have pit plugs, the function of which has not been extensively studied (Pueschel 1977, Scott et al. 1988, Ueki et al. 2008). Green plants (land plants and some green algae) and brown algae possess plasmodesmata (PD). PD are cytoplasmic continuities of adjacent cells in which plasma membranes are directly connected. It has been reported that various micro- and macromolecules can be transported via PD in green plants such as inorganic ions, metabolic products, proteins and RNAs (Kim 2005). It is also known that plant viruses spread through PD during

their infection (Carrington et al. 1996, Lough et al. 1998, Epel 2009).

In green plants, many ultrastructural studies on PD have been published, using TEM (Robards 1968, Fraster and Gunning 1969, Kwiatkowska and Maszewski 1986, Ding et al. 1992a, b, Botha et al. 1993, Franceschi et al. 1994, Volk et al. 1996, Cook et al. 1997). The most characteristic structural feature of PD in land plants is that they have appressed ER called desmotubule (Robards and Lucas 1990). Several other works noted additional internal substructures (Ding et al. 1992b, Badelt et al. 1994, Overall and Blackman 1996). Recently, PD-associated proteins have been identified in charophycean algae and land plants (White et al. 1994, Blackman and Overall 1998, Gestel et al. 2003, Faulkner et al. 2005, Sagi et al. 2005, Thomas et al 2008, Simpson et al. 2009, Faulkner and Maule 2010). These works suggested that there are highly complicated control mechanisms underlying the cell-to-cell molecular traffic via PD.

According to studies in green plants, i.e. land plants and some green algae, two types of PD can be distinguished, based on the timing of their formation or morphology (Hepler 1982, Franceschi et al. 1994, Ehlers and Kollmann 2001, Faulkner et al. 2008): the primary PD that are formed during cytokinesis, and the secondary PD that are produced after cytokinesis. It has been hypothesized that ER trapped between cell plate patches, creates the PD pore (Hepler 1982, Staehelin and Hepler 1996). The secondary PD are produced by modification of the primary PD or by post-cytokinetic *de-novo* formation, often giving rise to multiply-branched complex PD (Lucas et al. 1993).

Contrary to green plants, information on the structure of PD in brown algae has been limited (Marchant 1976). Among them, long-distance translocation of various substances through PD and pores of sieve elements of kelps was studied with

ultrastructures of these connections (Schmitz 1981, 1990), in *Laminaria groenlandica* Rosenv., *Alaria marginata* Postels & Ruprecht, *Nereocystis luetkeana* (K. Mertens) Postels & Ruprecht, *Laminaria hyperborea* (Gunnerus) Foslie and *L. saccharina* (Linnaeus) Lamouroux (Schmitz and Strivastava 1974, 1975, 1976, Schmitz and Kuhn 1982). Importantly, these studies on laminarialean plants and other brown algae (Bisalputra 1966, La Claire 1981, Katsaros and Galatis 1988) confirmed that PD in brown algae are simple without desmotubule, different from the case of land plants, except of one figure of *L. groenlandica* (Fig. 18 in Schmitz and Strivastava 1974). Pores in cross wall of sieve elements in laminarialean plants have more larger diameter, 100 – 400 nm in *N. luetkeana* (Schmitz and Strivastava 1976) and these are considered to be specialized structures for translocation of substances in sieve elements of large kelps (Schimitz 1990). These pores seem to be formed by enzymatic digestion of parts of the walls having PD (Marchant 1976).

In the brown alga, *Cutleria cynlindrica*, it was reported that PD-like structures appeared in the furrowing partition membrane during cytokinesis (La Claire 1981). A recent ultrastructural study on cytokinesis of several brown algae also revealed PD-like structures in the nascent cell partition membrane (Katsaros et al. 2009). Therefore, these reports suggest existence of the primary PD in brown algae. Detailed ultrastructural studies on cytokinesis of brown algae using rapid freezing/freeze substitution have been conducted (Nagasato and Motomura 2002, 2009, Katsaros et al. 2009, Nagasato et al. 2010). This technique revealed that novel membranous structures called “flat cisternae” (FCs), together with Golgi vesicles (GVs), contribute to partition membrane formation during cytokinesis, in a mode different from that of the phragmoplast-cell plate system of land plants (Schopfer and Hepler 1991, Samuels et al. 1995), Thus, the primary PD in

brown algae seem to be formed by a distinct process compared to that of green plants.

Electron tomography, which is a powerful electron microscopic technique for getting a nano-scale three-dimensional analysis, has been used in the ultrastructural studies of cytokinesis of land plants (Otegui and Staehelin 2004, Segui-Simarro et al. 2004, Haas and Otegui 2007). This technique will be also useful for analysis of tiny PD structure, in order to investigate their ultrastructure and the process of their formation. The present study investigated the ultrastructure of PD and the process of their formation in the brown alga *Dictyota dichotoma* using the conventional electron microscopy and electron tomography, based on rapid freezing and freeze-substitution.

Materials and Methods

Culture

Sporophytes of *Dictyota dichotoma* were collected by Dr. Kei Kimura, at Charatsunai, on the coast in front of Muroran Marine Station, Field Science Center for Northern Biosphere, Hokkaido University, Japan (42°19'N, 140°59'E). Culture was started from the apical parts on October, 2007. They were cultured in half-strengthened PES medium (Provasoli 1968) at 20°C long day condition (14 h light, 10h dark, photon flux density: 20 μmol・m^{-2}・s^{-1}).

Electron microscopy

Cultured material from 2 to 3 h after the end of the light period was used for cryofixation. Procedures for cryofixation and embedding methods were adopted from previous reports (Nagasato and Motomura 2002, Ueki et al. 2008). Apical parts of thalli (3 mm from the apex) were cut and put on formvar-coated gold loops (5 - 10 mm in

diameter), rapidly frozen by transferring the loop into liquid propane previously cooled to -180°C by liquid nitrogen. They were then immediately transferred to liquid nitrogen. Afterwards, the samples were transferred into cooled acetone (-80°C) containing 4% osmium tetroxide and stored at -80°C for about 2 days. The samples were gradually brought to room temperature as according to the following schedule: -20°C for 2 h, 4°C for 2 h and room temperature for 1 h. They were washed several times with acetone at room temperature and *en bloc* stained with 2% uranyl acetate in a mixture of methanol and acetone (volume ratio = 1 : 2) in ice bath for 1 h. Then, they were washed several times with a mixture solution of methanol and acetone (volume ratio = 1:2) and finally washed with acetone. They were infiltrated with Spurr's epoxy resin at room temperature as following : 20% resin in acetone for 12 h, 30% resin for 5 h, 40% for 5 h, 50% for 12 h, 70% for 5 h, 80% for 5 h, 100% for 2 days. From 80 to 100%, infiltration was carried out in desiccators. Samples were finally embedded in Spurr resin on dishes of aluminum foil. Ultrathin sections (80 - 100 nm) were cut using a diamond knife (Diatome, Hatfield, PA, USA) on an ULTRACUT ultramicrotome (Reichert-Jung, Depew, NY, USA) and mounted on formvar-coated copper slot grids. Sections were stained with 4% uranyl acetate and Reynolds' lead citrate (Reynolds 1963), and observed with a JEM-1011 electron microscope (JEOL, Tokyo, Japan).

Sample preparation for electron tomography

For observation with 300 kV electron microscope (Hitachi H9500 in Osaka University), 200 to 300 nm-thick sections were made. They were mounted on formvar-coated slot grids and stained with 4% uranyl acetate at 70°C for 1 h and lead citrate at room temperature for 10 min. After staining, the sample side of grids was also

coated by formvar membrane to sandwich the section. Then, 15-nm colloidal gold particles were attached on both sides of the grids. For observation with 2,000 kV electron microscope (Hitachi H3000 in Osaka University), 500 to 700 nm-thick sections were cut. The sections were floated on hot distilled water in order to remove wrinkles of sections. They were mounted on formvar-coated slot grids and stained with 2% uranyl acetate in 70% ethanol in microwave for 30 sec. After keeping them in dark for 20 min, they were stained with Sato's lead citrate (Sato 1968) in the microwave for 30 sec. After sandwich with formvar membrane, 20 nm colloidal gold particles were attached on both sides. Then, they were coated with carbon on both sides of the grid. These samples were subjected to acquisition of tilted images for tomographic analysis.

Image acquisition and tomographic analysis

200 to 300 nm-thick sections on the tilt-rotate specimen holder were observed with H-9500 (Hitachi, Tokyo, Japan) at 300 kV accelerate voltage. Images were acquired at magnification of 12,000 or 20,000 from -60^{o} to +60^{o} at 1^{o} intervals by F224HD CCD camera (TVIPS, Gauting, Germany) with the resolution of which was 2,048 x 2,048 pixels at a pixel size of 1.54 nm and 0.92 nm, respectively. Both single- and dual-axis electron tomography was performed. Dual-axis electron tomography was done at about two orthogonal axes in order to obtain high resolution images or reduce missing wedge artifact (Mastronarde 1997).

Similarly, sections on the tilt-rotate specimen holder were observed with H-3000 (Hitachi, Tokyo, Japan) at 2,000 kV accelerate voltage. Images were acquired at the magnification of 10,000 or 15,000 from -60^{o} to +60^{o} at 1^{o} intervals by F486BK CCD camera (Hitachi, Tokyo, Japan) with the resolution of which was 4,096 x 4,096

pixels at a pixel size of 3.45 nm and 2.23 nm, respectively. Both single- and dual-axis electron tomography was performed. Frame of each image was removed into 4,028 x 3774 pixels using Photoshop software (Adobe system Inc., San, Jose, CA, USA). The size of images was further binned into half (2,014 x 1887 pixels) by bicubic interpolation. All images were taken at the Research Center for Ultra-High Voltage Electron Microscopy (Osaka University, Osaka, Japan).

Tomograms were reconstructed by aligning each set of tilted images using gold particles as fiducial markers. All tomograms were analyzed using IMOD software (Kremer et al. 1996). The "SLICER", which is one of the programs packaged in IMOD, was used to extract slices by setting the rotation angles about the axes x, y and z, respectively. Three-dimensional models were drawn by tracing membranous structures using "3DMOD", which is the graphics component of IMOD, or "ISOSURFACE", which is an automatically drawing program packaged in IMOD. Volumes of objects were calculated using object meshes and "IMODINFO", which is one of the programs packaged in IMOD. For analysis of the frequency of occurrence of tubular membranous structures just nearby thinner and thicker cell wall regions, their volumes were calculated by extracting boxes of 0.924 x 0.200 x 0.154 μm^3 along the cell wall including the thinner and thicker regions. The volumes of cell wall regions were also calculated. Finally, the values were averaged from three part with the standard deviation and the frequency of occurrence was shown as the volumes of membranous structures per 0.028 μm^3 box.

Immunoelectron microscopy and cellulase-gold labeling

The cryofixation was performed as described above. Cryofixed materials were

transferred into cooled ethanol (-80°C) containing 0.2% glutaraldehyde and stored at -80°C for about 2 days. The samples were brought to room temperature as following: -20°C for 2 h, 4°C for 2 h and room temperature for 30 min. After washing several times with ethanol at room temperature, samples were infiltrated with Lowicryl HM20 resin at -30°C as following: 10% resin in ethanol for 5h, 20% for 12 h, 30% for 5 h, 50% for 5 h, 70% for 12 h, 80% for 5 h, 100% for 2 days. Embedding was done in TAAB Embedding Capsules using UV polymerizer under UV light for 2 days at -30^{o}C and for another 1 day at room temperature. Ultrathin sections (80-100 nm) were cut using a diamond knife on an ULTRACUT ultramicrotome and mounted on formvar-coated nickel slot grids.

Sections on formvar-coated nickel grids were floated on a 10 µL drop of PBS (137 mM NaCl, 2.7 mM KCl, 4.9 mM Na_2HPO_4, 1.5 mM KH_2PO_4, pH 7.4) for 10 min at room temperature, followed by incubation on blocking solution (2.5% skimmed milk, 5% normal goat serum and 0.05% NaN_3 in PBS) for 30 min or 1 h at 37°C. Afterwards, they were treated with a rabbit polyclonal anti-alginate antibody (Chi et al. 1999, Nagasato et al. 2010) diluted 1:1,000 in PBS overnight at 20°C in dark. For the control experiments, the primary antibody was omitted, or the sample was preincubated with 1 mg·mL^{-1} alginate (sodium salt, SIGMA Chemical, Saint Louis, MO, USA) in PBS for 1 h at 37°C. After washing with PBS for 10 min at room temperature, the specimens were treated with the secondary antibody, a goat anti-rabbit IgG conjugated with 15 nm colloidal gold particles (BBInternational, Cardiff, UK) for 1 h at 37°C. After washing with distilled water for 10 min at room temperature, the grids were stained with 4% uranyl acetate.

Cellulase from *Trichoderma reesei* (SIGMA Chemical, Saint Louis, MO,

USA) was conjugated to colloidal gold particles according to Samuels et al. (1995) and Nagasato et al. (2010) with a little modification. The pH of 10 nm colloidal gold solution (BB International) was adjusted to 4.9 with HCl. Five μL of 2 $mg \cdot mL^{-1}$ cellulase in distilled water was added to 500 μL of 10 nm colloidal gold and incubated in an ice bath for 5 min with stirring. Then, 25 μL of 1% polyethylene glycol (PEG 4,000, Merck, Darmstadt, Germany) was added for stability. The cellulase-gold conjugates were centrifuged at 14,000 rpm (Kokusan RM-190, Tokyo, Japan) for 90 min at 4°C. The resultant mobile pellet was transferred into a new microtube and 0.05 M citrate buffer (pH 4.9) was added up to 500 μL, followed by centrifugation at 14,000 rpm for 90 min at 4°C. The mobile pellet was transferred into a new microtube as the concentrated solution, and it was diluted 1 : 10 in 0.05 M citrate buffer for working solution.

Sections on formvar-coated nickel grids were floated on a 10 μL drop of 5% H_2O_2 for 10 min at room temperature, followed by treating with blocking solution for 20 min at room temperature. After washing with distilled water for 5 min at room temperature, they were rinsed with 0.05 M citrate buffer for 10 min at room temperature. Then, they were incubated with the cellulase-gold conjugate for 30 min at 37°C. After washing with citrate buffer for 5 min and distilled water for 5 min at room temperature, they were stained with 4% uranyl acetate.

Results

Observation of PD using conventional TEM

In *Dictyota dichotoma*, the usual thickness of mature cell walls of epidermal cells was around 0.5 μm (Fig. 1A). Simple, unbranched PD perforated the cell walls at

places where the cell wall thickness was much less, i.e. about 0.1 μm (Fig. 1B, C). In addition to the boundaries between epidermal cells, PD could be observed in cell walls separating epidermal and medullary cells. Electron-dense cell wall materials were densely packed in the thinner cell wall region, in which PD gathered to form a pit field (Fig. 1D, E). There was an electron-lucent sleeve between PD and surrounding electron-dense cell wall (Fig. 1D. E). The plasma membrane was continuous along PD to interlink the cytoplasms of adjacent cells through PD lumen. Different from the case of land plants, ER (desmotubule) was never observed in PD of *D. dichotoma* (Fig. 1F). On the contrary, tubular and other membranous structures in the cytoplasm were closely associated with the pit field (Fig. 1B). In a transverse view of PD, the inner diameter of the canal was from 10 to 20 nm (Fig. 1G). Instead of a desmotubule in the canal of PD, tiny electron-dense internal bridges were often observed (Fig. 1G). They appeared to extend from inner plasma membrane to the central portion in PD. In the sleeve around PD, electron-dense spokes were observed from the plasma membrane to the surrounding cell wall (arrowhead in Fig. 1G).

Observation of PD using electron tomography

Electron tomographic analysis showed a three-dimensional view nearby the pit field (Fig. 2). When a longitudinal section of pit fields was used for the image acquisition (Fig. 2A), it was confirmed that membranous structures were localized just beneath pit fields (Fig. 2B). They were not vesicles, but tubular structures which were sometimes branched (arrowheads in Fig. 2C, D). The frequency of occurrence of the membranous structures was compared between pit field and non-pit field regions by quantitative analysis. Volumes of the modeled membranous structures and cross wall

were calculated by extracting 0.028 μm^3 box along the cell wall corresponding to thinner (I, III, V in Fig. 2A) and thicker (II, IV, VI in Fig. 2A) regions. The volumes of membranous structures and cross wall were 0.00146 ± 0.00012 μm^3 and 0.00530 ± 0.00035 μm^3, respectively in the thinner cell wall regions, while 0.00053 ± 0.00020 μm^3 and 0.01249 ± 0.00075 μm^3, respectively in the thicker cell wall regions. These results indicated that localization of membrane structures was closely related to pit field. Some parts of them fused to the plasma membrane (Fig. 2E, F). When a glancing section of a pit field was used for the image acquisition (Fig. 2G), those membranous structures formed a complex network (Fig. 2H - J). Furthermore, slicer-tilted images displayed electron-dense internal bridges within PD (Fig. 2K - M).

PD formation during early stage of cytokinesis

Cytokinesis of *D. dichotoma* was investigated in order to clarify the process of PD formation. At the beginning of cytokinesis, FCs and GVs were arranged along the cytokinetic plane (Fig. 3A, B). At that time, patches of membrane sacs (MSs) began to be formed. PD-like perforations with a diameter of about 20 nm appeared in the MS (Fig. 3B). It was assumed that these tubular microcanals would be precursor structures of PD, i.e. pre-plasmodesmata (PPD). Observation of serial sections of MS (Fig. 3C - G) revealed initial funnel-shaped membrane protrusions from the membrane of MS (Fig. 3D), which would develop more advanced ones (Fig. 3E, F). Although ER membranes could be observed nearby the cytokinetic plane, they were never entrapped among MS patches, contrary to the case of land plants.

The structure of the developing MS was analyzed by electron tomography (Fig. 4A). A number of FCs and GVs were closely associated with MS, which appears to be

at the same stage of cytokinesis to that of Fig. 3. Slicer-tilted images showing a transverse view of MS indicated that PPD were not just membrane gaps on the nascent new cell partition membrane but tubular microcanals with an inner diameter of about 20 nm (Fig. 4B). Many PPD were unevenly formed in a restricted region of the MS to create PPD-rich and PPD-free regions. In the longitudinal view of PPD, electron-dense deposits could be observed at the outer surface of the central part in some PPD (Fig. 4A, insert).

Involvement of PD in the initial development of cell wall during cytokinesis

At more advanced stage of cytokinesis, a new cell partition membrane had completed and numerous PPD could be observed there (Fig. 5A). The average thickness of the diaphragm was about 70 nm, which was quite thinner than that of the mature cell wall. Tomographic observations revealed an electron-dense material accumulated on the central portion of the outer surface of PPD, from which a thin-layered electron dense material began to extend along the middle space of the diaphragm (Fig. 5B). The tomographic slices grazing to the diaphragm showed its distinct differentiation into PPD-rich and PPD-free regions (Fig. 5C). The slices extracted from the middle part of the diaphragm show that these electron dense materials originating from one PPD fused to those of neighboring PPD and finally extended over the PPD-rich region (Fig. 5D). At the same time, they spread out to the PPD-free region. It was assumed that the electron-dense material would be a nascent cell wall component.

By the progress of cytokinesis, this component was further extended in the diaphragm (Fig. 6A). It should be noted that the thickness of the diaphragm corresponding to the PPD-rich region became increased (average: 110 nm), similar

thickness to that of the mature cell wall of pit field areas (Fig. 6B, Fig. 1A-C). On the contrary, there was not such a thickening in the diaphragm corresponding to the PPD-free regions (average: 80 nm, Fig. 6C). Three-dimensional models made from sections illustrated that the cell wall synthesis was more advanced in the PPD-rich region (Fig. 6D), while it was delayed in the PPD-free region (Fig. 6E).

Localization of alginate and cellulose

Localization of alginate and cellulose was examined using immuno-electron microscopy and the specific enzyme binding-colloidal gold labeling, respectively. Gold particles were frequently detected on the thick cell walls when the anti-alginate antibody was used (Fig. 7A). Control experiment by pre-incubation of the primary antibody with alginate showed few or no gold particles on the cell wall (Fig. 7B). Apart from mature cell walls, localization of alginate was examined during cytokinesis. Alginate could be detected in the young MS (Fig. 7C). Moreover, alginate was detected in the thickening pit field of the later stages (Fig. 7D, E). Colloidal gold-conjugated cellulase probe highly labeled the thick cell walls, suggesting the presence of cellulose (Fig. 7F). In contrast to the case of alginate, cellulose could not be detected during early stage of developing cell partition membrane (Fig. 7G, H), but the cellulase probe gradually started labeling the cell wall (Fig. 7I) with the diaphragm development.

Discussion

Ultrastructure of plasmodesmata in brown algae

The detailed analysis of PD ultrastructure made by TEM in the present study revealed that *D. dichotoma* possesses ER-free, simple PD with an inner diameter of

10-20 nm. The continuity of the plasma membrane along the entire canal indicated that PD provide the functional cytoplasmic connections for the cell-to-cell communication. Moreover, this study identified plasmodesmatal substructures in *D. dichotoma*, the internal bridges. In land plants, there have been many reports of plasmodesmatal internal components at the ultrastructural level (Ding et al. 1992b, Botha and Cross 2000), i.e. a desmotubule passing through the entire canal (Robards and Lucas 1990), particular structures on the inner plasma membrane and on the outer membrane of the desmotubule, and spoke-like extensions. In green algae, globular structures were also observed filling the inner space within PD (Fraster and Gunning 1969). In *D. dichotoma*, based on the observation of transverse ultrathin sections, electron-dense internal bridges directly elongate from the inner plasma membrane to the central point in PD. Electron tomographic analysis also revealed them. Considering the pixel size used in the tomogram (1.54 nm), it was concluded that the internal bridges were not a "superimposed" structure but an actual internal structure. However, it is still unclear whether they are present in the entire canal because the present tomographic analysis could not obtain a clear image of the central portion of PD. This may be caused by that the central portion of PD was surrounded by electron-dense cell wall material. In the ultrathin sections, internal bridges in PD were not always observed. This presumably suggests that they may not fill the whole canal, unlike the plasmodesmatal substructures of land plants. Although the PD structure of the brown alga *D. dichotoma* was not as complex as that of green plants, it is speculated that internal bridges would have a similar function in the intercellular traffic of a variety of molecules. By bridging the plasma membrane of the canal, they can physically limit the size of the cytoplasmic space through which the molecules can freely move. In green plants, there have been

reports on the relationship between the size of the cytoplasmic space and the size exclusion limit which is the maximum molecular weight to pass through the PD (Citovsky 1993, Lucas and wolf 1993, Cook et al. 1997). At present, it is still unknown how and what molecules can be actually transported through the brown algal PD. It requires further work including the molecular components of PD of brown algae.

In *D. dichotoma* tubular membranous structures beneath the plasma membrane well developed nearby pit field as described in the laminarialean plants (Schmitz and Kuhn 1982). They exhibited a similar electron density and thickness with the plasma membrane. Both conventional TEM observations and electron tomography clearly showed that some parts of them fused to the plasma membrane. From closely localization this complex membranous network just beneath the pit field at where the cell wall became thinner, it may be suggested that they also take part in the cell-to-cell traffic via PD.

Primary plasmodesmata in brown algae

PD are categorized into two groups according to timing of their formation: the primary PD produced during cytokinesis, and the secondary PD formed post-cytokinetically (Maule 2008). Process of PD formation has been well studied in green plants. The most accepted model in land plants is that ER membranes are entrapped during the cell plate formation in cytokinesis and their physical obstructions consequently give rise to plasmodematal perforation in the cell plate (Hepler 1982). ER transversing the developing cell plate has been also reported in some Charophycean algae (Pickett-Heaps 1967, Cook et al. 1997). Contrary to land plants, there is limited information available about when, where and how brown algal PD are produced. The

present study revealed that PD formation in vegetative cells of *D. dichotoma* takes place during cytokinesis with membrane protusions into MSs. At the early stages of their formation, structures called pre-plasmodesmata (PPD) were found, showing particular features, i.e. (1) they were tubular micro-canals with almost the same size (20 nm) with the mature PD, (2) they were evenly located at certain areas in the MSs and persisted after completion of the cell partition membrane, and finally (3) they were formed in the sites of "future" pit fields. Similar perforations in the cytokinetic diaphragm have been described in *Cutleria cylindrica*, *Halopteris congesta*, *Sphacelaria rigidula*, and *Dictyota dichotoma* (La Claire 1981, Katsaros and Galatis 1985, Katsaros et al. 2009).

Nagasato and Motomura (2002) and Nagasato et al. (2010) reported that PD formation could be hardly detected during the first cytokinesis in zygotes of brown algae, *Scytosiphon lomentaria* and *Silvetia babingtonii*. However, PD can be frequently detected in the cell walls of more developed thalli in *S. lomentaria* and *Fucus distichus*, especially as a pit field in *F. distichus* (unpublished data). From the above observations it may be suggested that apart from the primary PD formation found in the present study, PD may be formed secondarily in brown algae.

PD gather to form pit fields in distinct sites of the cell wall in *D. dichotoma*. Similarly, pit fields were arranged in the periphery of the cortical cells of *Laminaria hyperborea* and *L. saccharina* (Schmitz and Kuhn 1982). From the present study, we speculate that PPD formation and the following pit field formation are occurred during cytokinesis in the brown algae and position of the pit field will be turned out with cell expansion and thallus morphogenesis. Actually, it was found that position of nascent pit field with densely gathering of PPD on inner side of of *Dictyota* epidermal cells is almost corresponded to it of the "mature" pit fields of the epidermal cells (data not

shown).

Involvement of plasmodesmata in the initial cell wall development

In the present study, it was also found that formation of PPD will be coupled with the initial cell wall development in *D. dichotoma*. During cytokinesis, an electron-dense material started accumulating on the outer surface of the middle point of PPD and further elongate from PPD-rich regions to PPD-free ones, and finally it filled through the cell partition membrane at the end of cytokinesis as cell wall. Electron tomographic analysis clearly demonstrated that the electron-dense material was indeed accumulated on the lateral middle surface of PPD. In brown algae, the cell wall is composed of cellulose, acidic polysaccharides including alginate and sulfated fucans, phenolic compounds and proteins (Kloareg and Quatrano1988, Schoenwaelder and Clayton 1999). The candidate for the skeletal cell wall components in brown algae would be cellulose and alginate because sulfated fucans consist of non-crystallized matrix components (Kloareg and Quatrano1988). The previous (Nagasato et al. 2010) and present studies clearly showed that cellulose deposition took place after completion of cytokinesis. Nagasato et al. (2010) also reported that GVs containing fucoidan firstly fused to flat cisternae during cytokinesis of *Silvetia* zygotes, and afterwards, these developed to expanded FCs, membranous network and MS. Then, alginate could be detected in MSs, although there were few PD in the septum in *Silvetia* zygotes. Kloareg and Quatrano (1988) reported that the cell wall of *Dictyota* contained ascophyllans and glycuorono- fucogalactans as sulfated fucans, instead of fucoidans, therefore, in this study, we could not detect deposition patterns of these sulfated fucans during cytokinesis of *D. dichotoma* using monoclonal anti-fucoidan antibody. However,

considering the non-crystallized cell wall matrix of sulfated fucans, a thin-layered electron dense cell wall materials elongating from the middle part of PPD in MSs during cytokinesis would be alginate, which was also supported by immuno-electron microscopy using anti-alginate antibody. PD formation might be linked to alginate synthesis during cytokinesis in *D. dichotoma*. However, further molecular and cytological studies will be necessary to clarify the role of PD in brown algae.

Acknowledgements

We would like to express our thanks to Dr. K. Kimura, National Research Institute of Fisheries and Environment of Inland Sea, Fisheries Research Agency, for using culture materials of *Dictyota dichotoma*. This study was supported by a Grant-in-Aid for Scientific Research from the Ministry of Education, Science and Culture, Japan, and Research Fellow of the Japan Society for the Promotion of Science (20370025, 22370024, 22570084). A part of this work was supported by "Nanotechnology Network Project of the Ministry of Education, Culture, Sports, Science and Technology (MEXT), Japan" at the Research Center for Ultrahigh Voltage Electron Microscopy, Osaka University (Handai multi-functional Nano-Foundry).

References

Badelt K, White RG, Overall RL, Vesk M (1994) Ultrastructuralspecializations of the cell-wall sleeve around plasmodesmata. Am J Bot 81:1422–1427

Bisalputra T (1966) Electron microscopic study of the protoplasmic continuity in certain brown algae. Can J Bot 44:89-93

Blackman LM, Overall RL (1998) Immunolocalisation of the cytoskeleton to plasmodesmata of *Chara coralline*. Plant J 14:733-741

C. E.J. Botha CEJ, Hartley BJ, Cross RHM (1993) The ultrastructure and computer-enhanced digital image analysis of plasmodesmata at the kranz mesophyll-bundle sheath interface of *Themeda triandra* var. *imberbis* (Retz) A. Camus in conventionally-fixed blades. Ann Bot 72:255-261

Botha CEJ, Cross RHM (2000) Towards reconciliation of structure with function in plasmodesmata-who is the gatekeeper? Micron 31:713-721

Carrington JC, Kasschau KD, Mahajan SK, Schaad MC (1996) Cell-to-cell and long-distance transport of viruses in plants. Plant Cell 8:1669-1681

Chi E-S, Henry EC, Kawai H, Okuda K (1999) Immunogold-labeling analysis of alginate distributions in the cell walls of chromophyte algae. Phycol Res 47:53-60

Citovsky V (1993) Probing plasmodesmatal transport with plant viruses. Plant Physiol 102:1071-1076

Cook ME, Graham LE, Botha CEJ, Lavin CA (1997) Comparative ultrastructure of plasmodesmata of Chara and selected bryophytes: toward an elucidation of the evolutionary origin of plant plasmodesmata. Amer J Bot 84 (9):1169-1178

Ding B, Haudenshield JS, Hull RJ, Wolf S, Beachy RN, Lucas WJ (1992a) Secondary plasmodesmata are specific sites of localization of the tobacco mosaic virus

movement protein in transgenic tobacco plants. Plant Cell 4:915-928

Ding B, Turgeon R, Parthasarathy MV (1992b) Substructure of freeze-substituted plasmodesmata. Protoplasma 169:28-41

Ehlers K, Kollmann R (2001) Primary and secondary plasmodesmata: structure, origin, and functioning. Protoplasma 216:1-30

Epel BL (2009) Plant viruses spread by diffusion on ER-associated movement-protein-rafts through plasmodesmata gated by viral induced host beta-1, 3-glucanases. Semin Cell Dev Biol 20:1074-1081

Faulkner C, Akman OE, Bell K, Jefree C, Oparka KJ (2008) Peeking into pit fields: a multiple twinning model of secondary plasmodesmata formation. Plant Cell 20:1504-1508

Faulkner CR, Blackman LM, Cordwell SJ, Overall RL (2005) Proteomic identification of putative plasmodesmatal proteins from *Chara coralline*. Proteomics 5:2866-2875

Faulkner C, Maule A (2010) Opportunities and successes in the search for plasmodesmal proteins. Protoplasma 248:27–38

Fernandez-Calvino L, Faulkner C, Walshaw J, Saalbach G, Bayer E, Benitez-Alfonso Y, Maule A (2011) Arabidopsis plasmodesmal proteome. Plos One 6:1-13.

Franceschi, VR, Ding B, Lucas WJ (1994) Mechanism of plasmodesmata formation in characean algae in relation to evolution of intercellular communication in higher plants. Planta 192:347-358

Fraster TW, Gunning BES (1969) The Ultrastructure of plasmodesmata in the filamentous green alga, *Bulbochaete hiloensis* (Nordst.) Tiffany. Planta 88:244-254

Gestel KV, Slegers H, von Witsch M, Samaj J, Baluska F, Verbelen JP (2003)

Immunological evidence for the presence of plant homologues of the actin related protein Arp3 in tobacco and maize: subcellular localization to actin-enriched pit fields and emerging root hairs. Protoplasma 222:45-52

Haas TJ, Otegui MS (2007) Electron tomography in plant cell biology. J Integr Plant Biol 49(8):1091-1099

Hepler PK (1982) Endoplasmic reticulum in formation of the cell plate and plasmodesmata. Protoplasma 111:121-123

Jo Y, Cho WK, Rim Y, Moon J, Chen XY, Chu H, Kim CY, Park ZY, Lucas WJ, Kim JY (2011) Plasmodesmal receptor-like kinases identified through analysis of rice cell wall extracted proteins. Protoplasma 248:191–203

Katsaros C, Galatis B (1985) Ultrastructural studies on thallus development in *Dictyota dichotoma* (Phaeophyta, Dictyotales). Eur J Phycol 20:263-276

Katsaros C, Galatis B (1988) Thallus development in *Dictyopteris membranacea* (Phaeophyta, Dictyotales). Br Phycol J 23:71–88

Katsaros C, Motomura T, Nagasato C, Galatis B (2009) Diaphragm development in cytokinetic vegetative cells of brown algae. Bot Mar 52:150-161

Kim JY (2005) Regulation of short-distance transport of RNA and protein. Curr Opin Plant Biol 8:45-52

Kloareg B, Quatrano RS (1988) Structure of the cell walls of marine algae and ecophysiological functions of the matrix of polysaccharides. Oceanogr Mar Biol Annu Rev 26:259-315

Kremer JR, Mastronarde DN, McIntosh JR (1996) Computer visualization of three-dementional image data using IMOD. J Struct Biol 116:71-76

Kumar NM, Gilula NB (1996) The Gap junction review communication channel. Cell

84:381-388

Kwiatkowska M, Maszewski J (1986) Changes in the occurrence and ultrastructure of plasmodesmata in antheridia of *Chara vulgaris* L. during different stages of spermatogenesis. Protoplasma 132:179-188

La Claire II JW (1981) Occurrence of plasmodesmata during infurrowing in a brown alga. Biol Cell 40:139-142

Lough TJ,Shash K, Xoconostle-Cázares B, Hofstra KR, Beck DL, Balmori E, Forster RLS, Lucas WJ (1998) Molecular dissection of the mechanism by which Potexvirus triple gene block proteins mediate cell-to-cell transport of infectious RNA. MPMI 11:801-814

Lucas WJ, Wolf S (1993) Plasmodesmata: the intercellular organelles of green plants. Trends Cell Biol 3:308-315

Lucas WJ, Ding B, van den Schoot C (1993) Plasmodesmata and the supracellular nature of plants. New Phytologist 12:435-476

Makowski L, Caspar DL, Phillips WC, Baker TS, Goodenough DA (1984) Gap junction structures. VI. Variation and conservation in connexon conformation and packing. Biophysical J 45:208-218

Marchant HJ (1976) Plasmodesmata in algae and fungi. *In* (B. E. S. Gunning and T. A. W. Robards, eds) *Intercellular Communication in Plants: Studies on Plasmodesmata*. Springer-Verlag, Berlin. Pp. 59-80

Mastronarde DN (1997) Dual-axis tomography: an approach with alignment mehods that preserve resolution. J Struct Biol 120: 343-352

Maule AJ (2008) Plasmodesmata: structure, function and biogenesis. Curr Op Plant Bio 11:680-686

Nagasato C, Inoue A, Mizuno M, Kanazawa K, Ojima T, Okuda K, Motomura T (2010) Membrane fusion process and assembly of cell wall during cytokinesis in the brown alga, *Silvetia babingtonii* (Fucales, Phaeophyceae). Planta 232:287-298

Nagasato C, Motomura T (2002) Ultrastructural study on mitosis and cytokinesis in *Scytosiphon lomentaria* zygotes (Scytosiphonales, Phaeophyceae) by freeze-substitution. Protoplasma 219:140-149

Nagasato C, Motomura T (2009) Effect of latrunculin B and brefeldin A on cytokinesis in the brown alga *Scytosiphon lomentaria* zygotes (Scytosiphonales, Phaeophyceae). J Phycol 45:404-412

Otegui MS, Staehelin LA (2004) Electron tomographic analysis of post-meiotic cytokinesis during pollen development in *Arabidopsis thaliana*. Planta 218:501-515

Overall RL, Blackman LM (1996) A model of the macromolecular structure of plasmodesmata. Trends Plant Sci 1:307–311

Pickett-Heaps JD (1967) Ultrastructure and differentiation in *Chara* sp. II. Mitosis. Aust J biol Sci 20:883-894

Provasoli, L (1968) Media and prospects for the cultivation of marine algae. *In*: (A. Watanabe and A. Hattori, eds) *Cultures and collections of algae*. Japanese Society of Plant Physiologists, Hakone. pp. 63-75

Pueschel CM (1977) A freeze-etch study of the ultrastructure of red algal pit plugs. Protoplasma 91:15-30

Reynolds ES (1963) The use of lead citrate at high pH as an electron-opaque stain in electronmicroscopy. J Cell Biol 17:208-212

Robards AW (1968) A new interpretation of plasmodesmatal ultrastructure. Planta 82:200-210

Robards AW, Lucas WJ (1990) Plasmodesmata. Annu Rev Plant Physiol Plant Mol Biol 41:369-419

Sagi G, Katz A, Gelbart DG, Epel BL (2005) Class 1 reversibly glycosylated polypeptides are plasmodesmal-associated proteins delivered to plasmodesmata via the Golgi apparatus. Plant Cell 17: 1788-1800

Samuels AL, Giddings TH, Staehelin LA (1995) Cytokinesis in Tobacco BY-2 and root tip cells: a new model of cell plate formation in higher plants. J Cell Biol 130:1345-1357

Sato, T. (1968) Lead citrate stain in electron microscopy. J Electron Microsc 17:158–159

Schmitz K (1981) Translocation. *In*: (C. S. Lobban and M. J. Wynne, eds) The biology of seaweeds. Blackwell Scientific Publications, Oxford. pp. 534-558

Schmitz K (1990) Algae. *In*: (H. D. Behnke and R. D. Sjolund, eds.) Sieve elements. Comparative structure, induction and development. Springer-Verlag. Pp.1-18

Schmitz K, Kuhn R (1982) Fine structure, distribution and frequency of plasmodesmata and pits in the cortex of *Laminaria hyperborea* and *L. saccharina.* Planta 154:385-392

Schmitz K, Srivastava, L (1974) Fine structure and development of sieve tubes in *Laminaria groenlandica* Rasenv. Cytobiologie 10:66-87.

Schmitz K, Srivastava, L (1975) On the fine structure of sieve tubes and the physiology of assimilate transport in *Alaria maginata*. Can J Bot 53:861-876

Schmitz K, Srivastava LM (1976) The fine structure of sieve elements of *Nereocystis lutkeana*. Amer J Bot 63(5):679-693

Schoenwaelder MEA, Clayton MN (1999) The presence of phenolic compounds in

isolated cell walls of brown algae. Phycologia 38:161-166

Schopfer CR, Hepler PK (1991) Distribution of membranes and the cytoskeleton during cell plate formation in pollen mother cells of *Tradescantia*. J Cell Sci 100:717-728

Scott J, Thomas J, Saunders B (1988) Primary pit connections in *Compsopogon coeruleus* (Balbis) Montagne (Compsopogonales, Rhodophyta). Phycologia 27:327-333

Segui-Simarro JM, Austin II JR, White EA, Staehelin LA (2004) Electron tomographic analysis of somatic cell plate formationin meristematic cells of *Arabidopsis* preserved by high-pressure freezing. Plant Cell 16:836-856

Simpson C, Thomas C, Findlay K, Bayer E, Maule AJ (2009) An Arabidopsis GPI-anchor plasmodesmal neck protein with callose binding activity and potential to regulate cell-to-cell trafficking. Plant Cell 21:581-594

Staehelin LA, Hepler PK (1996) Cytokinesis in higher plants. Cell 84:821-824

Thomas CL, Bayer EM, Ritzenthaler C, Fernandez-Calvino L, Maule AJ (2008) Specific targeting of a plasmodesmal protein affecting cell-to-cell communication. PLoS Biol 6:180-190

Ueki C, Nagasto C, Motomura T, Saga N (2008) Reexamination of the pit pulgs and the characteristic membranous structures in *Porphyra yezoensis* (Bangiales, Rhodophyta). Phycologia 47:5-11

Volk GM, Turgeon R, Beebe DU (1996) Secondary plasmodesmata formation in the minor-veinphloem of *Cucumis melo* L. and *Cucurbita pepo L.* Planta 199:425-432

Yoon HS, Hackett JD, Ciniglia C, Pinto G, Bhattacharya D (2004) A molecular timeline for the origin of photosynthetic eukaryotes. Mol Biol Evol 21:809-818

White RG, Badelt K, Overall RL, Vesk M (1994) Actin associated with plasmodesmata.

Protoplasma 180:169-184

Figure Legends

Fig. 1. Ultrastructure of PD of *D. dichotoma*. (**A**) Overview of an epidermal cell. Plasma membranes and cell organelles are well preserved by the rapid freezing/freeze-substitution. Arrow indicates a cell wall region containing many PD (pit field). (**B**, **C**) Enlargement of arrow region of (A). PD perforate thin cell wall with thickness of about 100 nm. At the vicinity of PD, membranous structures are observed (arrow). (**D**, **E**) Numerous PD gather in the cell wall to form a pit field. There is an electron-lucent sleeve between PD and surrounding cell wall. (**F**) Longitudinal view of a PD, which directly connect cytoplasm (CP) of adjacent cells. A desmotubule cannot be observed in the PD lumen. (**G)** Transverse views of PD. Inner diameter of the canal is generally 10-20 nm. Electron-dense structure (internal bridges, IB) are observed to extend from the plasma membrane within PD. Note spoke from the plasma membrane across the sleeve to cell wall (arrowhead). CW cell wall, IB internal bridge, IPM inner leaflet of the plasma membrane, OPM outer leaflet of the plasma membrane. Scale Bar: 2 μm (A), 200 nm (B,D), 20 nm (C,F,G,), 50 nm (E).

Fig. 2. Tomographic analysis of a pit field. Three sets of single-axis tomograms (**A - D**, **E – F, G - M**). (**A**) A 1.54 nm-thick tomographic slice. A longitudinal section of pit fields is used. Thinner (I, III, V) and thicker (II, IV, VI) cell wall regions were used for the quantitative analysis (see text). (**B**) Three-dimensional tomographic model depicted from (A). Pit fields (PT) are located in the thinner cell wall regions. (**C, D**) Tilted view of the model in B showing the upper side (**C**) and lower side (**D**) of the model. Note that tubular membranous structures are observed nearby pit fields, having branches (arrowheads). (**E**) A 2.23 nm-thick tomographic slice. A longitudinal section of the pit

field is used. (**F**) Longitudinal slicer views of the pit field encircled by the dotted rectangle in (E). Note that a part of the membranous structures is continuous from PM (arrow). Arrowheads indicate PD. (**G**) A 1.54 nm-thick tomographic slice. A glancing section of the pit field is used. (**H**) Transverse slicer view of the pit field. PD canals are visible within the cell wall. (**I**) Transverse slicer view of cytoplasmic region over the pit field. Well-developed membranous structures are recognized. (**J**) Three-dimensional tomographic model of the membranous structures in (I). They possess a intricate network. (**K - M**) Transverse slicer views of serial slices of PD. Internal bridges can be seen as observed (arrowheads). Chl chloroplast, G Golgi body, M mitochondria, N nucleus, Scale Bar: 500 nm (A - E, G, J), 200 nm (F, H, I), 20 nm (K - M).

Fig. 3. Structure of PPD. (**A**) Overview of a cell during the early stage of cytokinesis. Formation of cytokinetic plane is proceeding perpendicularly to the longitudinal axis of the cell. FCs are arranged on the cytokinetic plane (arrowheads). Several MSs are formed (arrows). (**B**) Enlargement of the MS shown by the right arrow in A. Note that tubular pre-plasmodesmata (PPD) appear in the MS (arrows). (**C - G**) Consecutive serial sections. Membrane protrusions can be seen in MS (arrowheads). Scale Bar: 1 μm (A), 100 nm (B-G).

Fig. 4. Tomographic analysis of PPD at an early stage of MS formation. A dual-axis tomogram. (**A**) A 2.23 nm-thick tomogram. Expanding MS with a gap (arrow). Inset shows a 2,23 nm-thick longitudinal slicer view of PPD. Note that electron-dense material is deposited on the outer surface of PPD (arrowhead). (**B**) Transverse slicer view of the MS encircled by the dotted rectangle in (A). A gap (arrow in A) can be

observed is in the center of the MS (arrow). Note that PPD are unevenly formed in MSs (arrowheads), resulting in PPD-rich (PR) and PPD-free regions (PF). PM plasma membrane. Scale Bar: 500 nm (A), 100 nm (B), 50 nm (inset in A).

Fig. 5. PPD in nascent diaphragm. A dual-axis tomogram. (**A**) A 2.23 nm-thick tomographic slice. A number of PPD are present in the nascent diaphragm. (**B**) Longitudinal views of PPD of 2.23 nm-thick tomographic slice. Note that electron-dense material deposited on the outer surface of the central portion of PPD and further extend to the middle space of cell partition membrane (arrows). Arrowheads indicate PPD. (**C**) Transverse slicer view of the cell partition membrane encircled by the dotted rectangle in (A). Distinct PPD-rich (PR) and PPD-free (PF) regions are observed. (**D**) Enlarged transverse slicer views of the cell partition membrane. Note extension of electron-dense material from PPD (arrows). Arrowheads indicate PPD. Chl chloroplast, FC flat cisterna, M mitochondria, N nucleus, V vacuole. Scale Bar: 500 nm (A), 100 nm (B, C, E, F), 200 nm (D).

Fig. 6. Tomographic analysis of an advanced stage of the cytokinetic diaphragm formation. A dual-axis tomogram. (**A**) A 1.54 nm-thick tomographic slice. A PPD-free region (PF) is located between two PPD-rich regions (PR). (**B**) Magnified image of the PPD-rich region shown in the upper left of (A). (**C**) Magnified image of the PPD-free region shown in the center of (A). (**D**) Three-dimensional tomographic model drawn from (B) using ISOSURFACE. The cell wall materials (arrow) develop well in the PPD-rich region . (**E**) Three-dimensional tomographic model drawn from (C) using ISOSURFACE. Development of the cell wall materials (arrow) is delayed in PPD-free

region. FC flat cisterna, M mitochondria, PF PPD-free region, PM plasma membrane, PR PPD-rich region, V vacuole. Scale Bar: 500 nm (A), 100 nm (B-E).

Fig. 7. Immunogold localization of alginate and cellulose. (**A**) Alginate is detected in the mature cell wall (CW), but not in the Golgi body (G). (**B**) Control with preincubation of the anti-alginate antibody with alginate. Note that there are only a few gold particles. (**C**) Alginate can be detected in MS. (**D**) Cell wall material starts depositing in the pit field where alginate can be detected nearby PPD . (**E**) Enlargement of D, showing gold particles near PPD (arrows). (**F**) Cellulose can be detected in the mature thick cell wall. (**G**) Just after the completion of the cell partition membrane, cellulose cannot be detected in it. (**H**) Cellulose is localized in the mother cell wall (MCW), but not in the nascent diaphragm. (**I**) Cellulose begin to be detected in more developed diaphragm. CW cell wall, G Golgi body, MCW mother cell wall, MS membranous sac. Scale Bar: 200 nm (A, B, C, D, H, I), 100 nm (E), 500 nm (F, G).

Fig.1

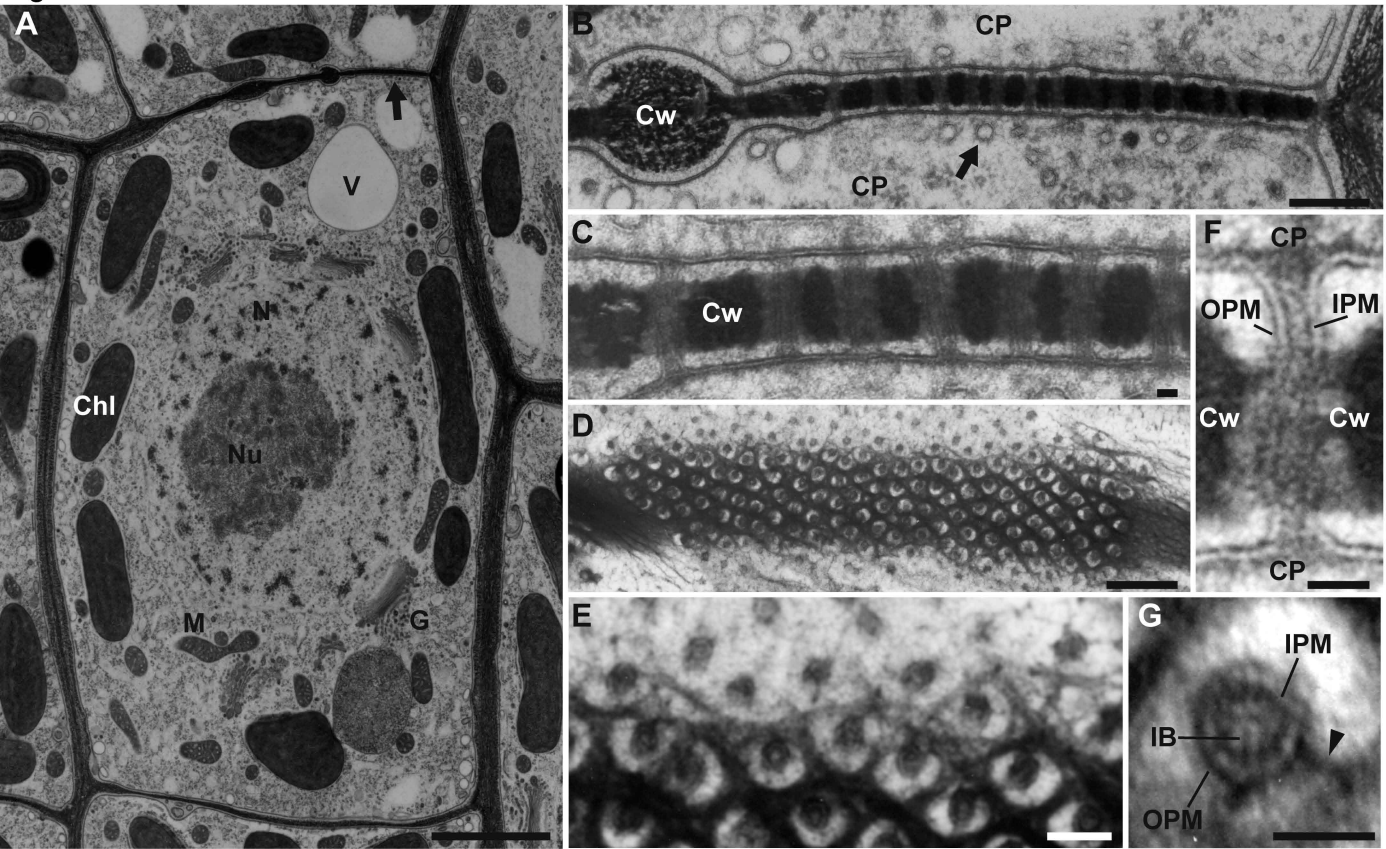

Fig.2

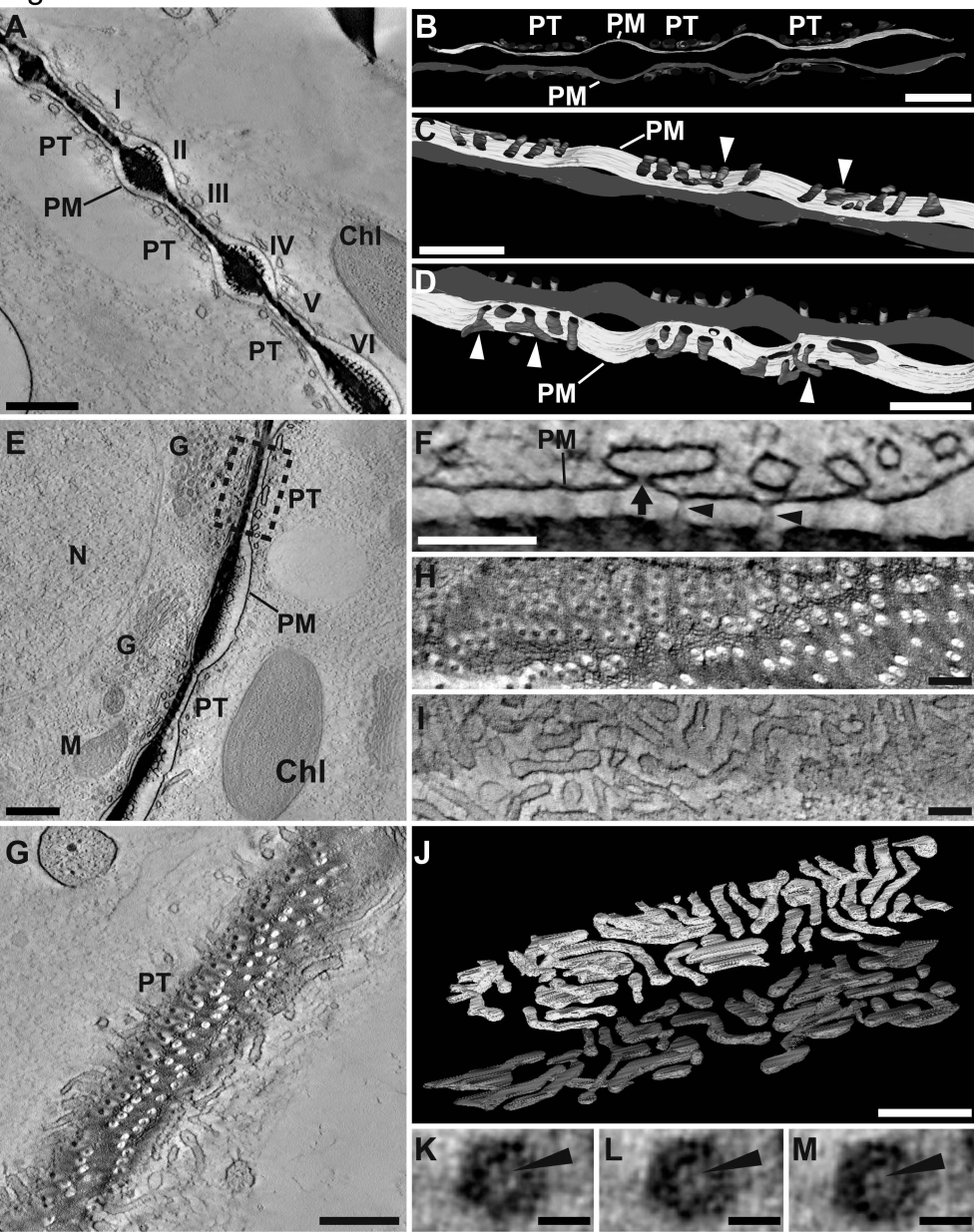
A
I
PT
II
PM
III
PT
IV
Chl
V
PT
VI
B
PT
PM
PT
PT
PM
C
PM
D
PM
E
G
PT
N
PM
G
PT
M
Chl
F
PM
H
I
G
PT
J
K
L
M

Fig.3

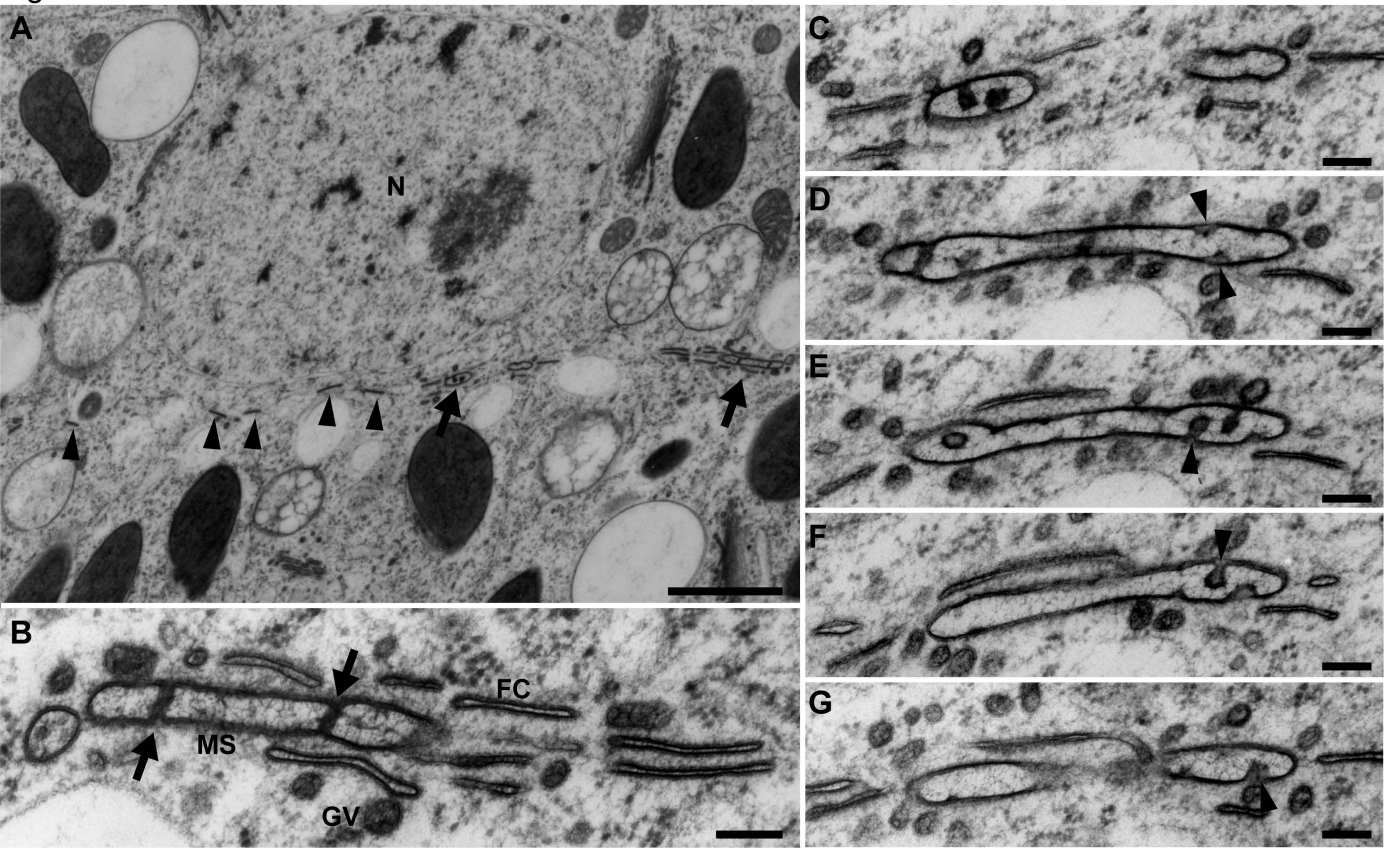

Fig.4

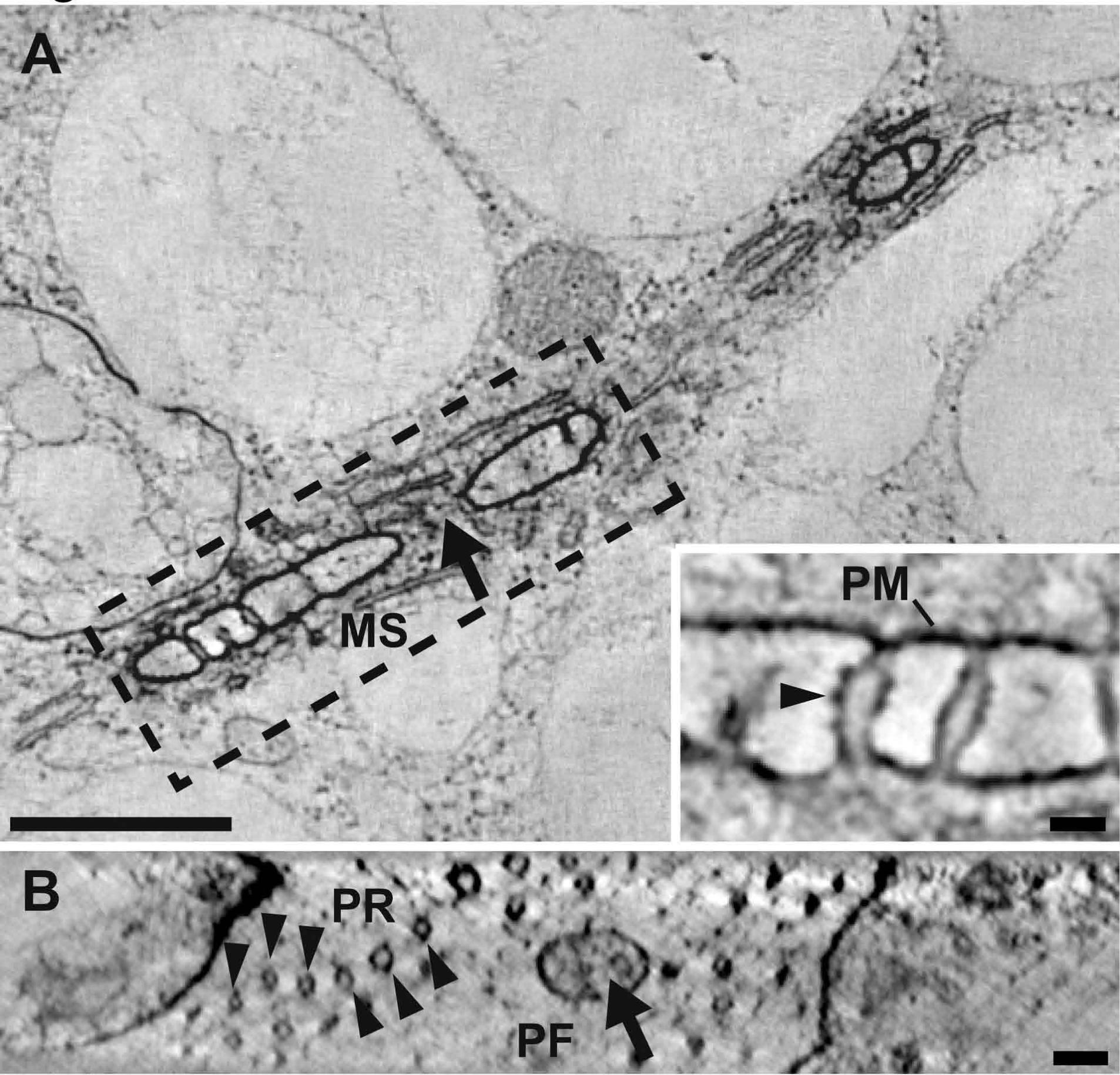

Fig.5

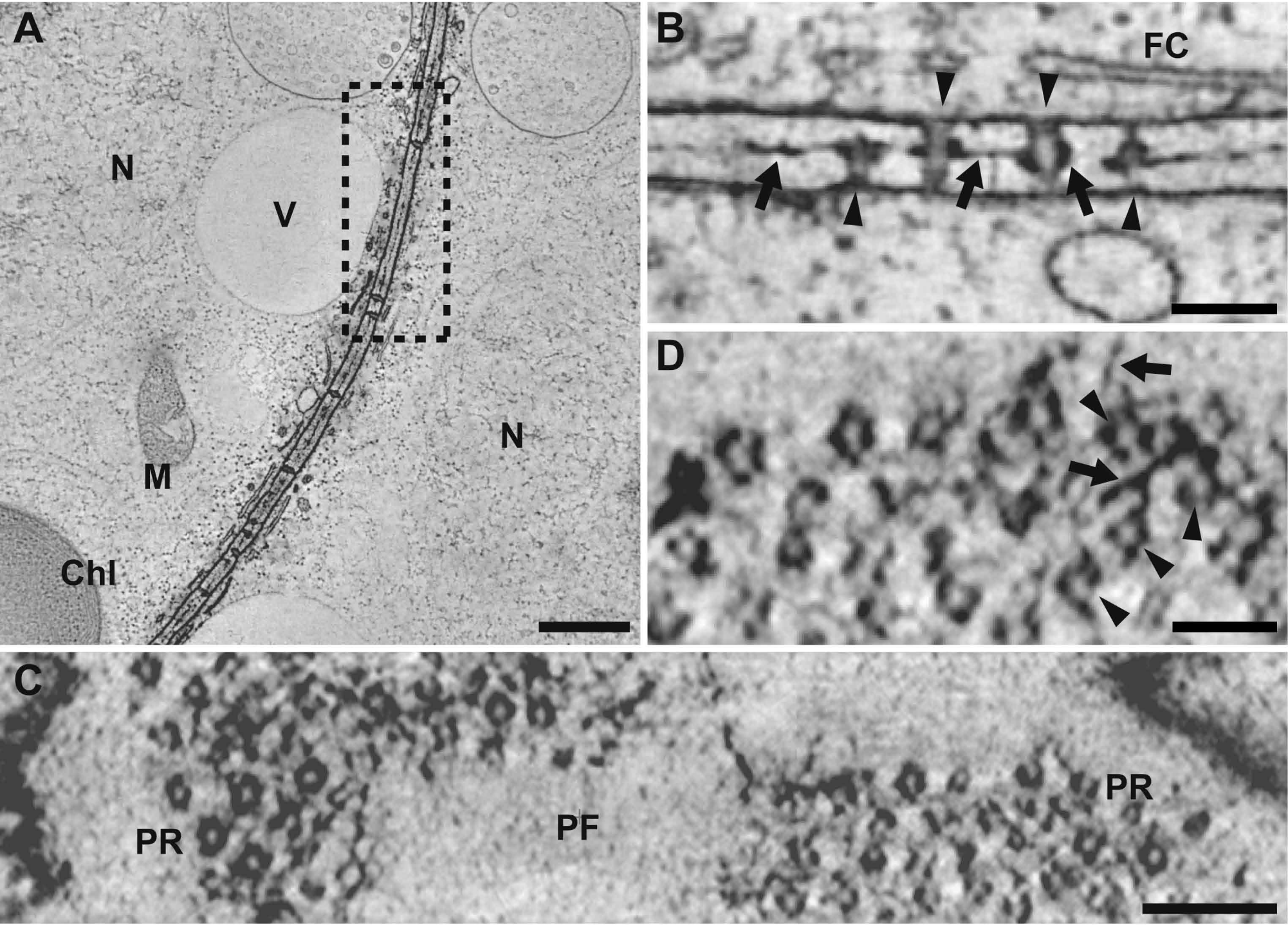

Fig.6

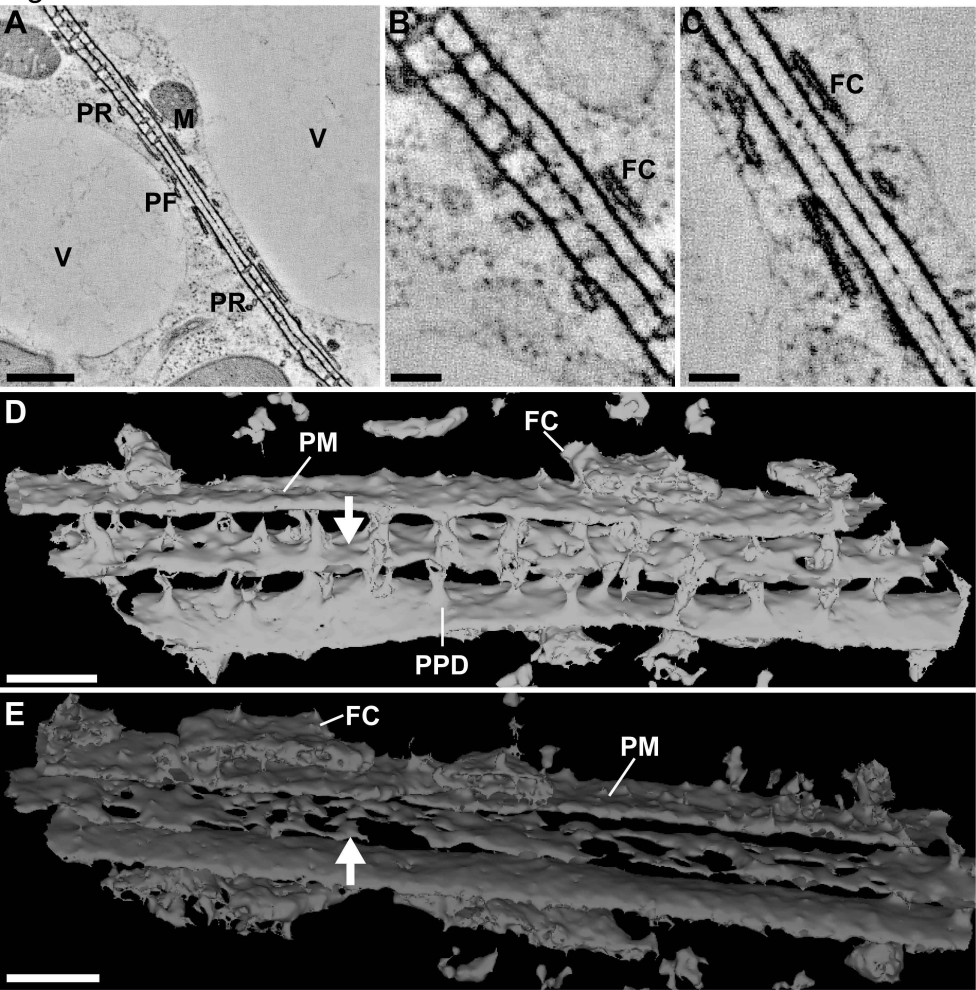

Fig7